Broadband cross-polarization conversion by symmetry-breaking ultrathin metasurfaces

Sha Hu, Shengyan Yang, Zhe Liu, Junjie Li, and Changzhi Gu

Citation: Appl. Phys. Lett. **111**, 241108 (2017);
View online: https://doi.org/10.1063/1.5006540
View Table of Contents: http://aip.scitation.org/toc/apl/111/24
Published by the American Institute of Physics

Broadband cross-polarization conversion by symmetry-breaking ultrathin metasurfaces

Sha Hu,[1,2] Shengyan Yang,[1,2] Zhe Liu,[1] Junjie Li,[1,2] and Changzhi Gu[1,2,3,a)]
[1]*Beijing National Laboratory for Condensed Matter Physics, Institute of Physics, Chinese Academy of Sciences, Beijing 100190, China*
[2]*School of Physical Sciences, CAS Key Laboratory of Vacuum Physics, University of Chinese Academy of Sciences, Beijing 100049, China*
[3]*Collaborative Innovation Center of Quantum Matter, Beijing 100190, China*

(Received 26 September 2017; accepted 30 November 2017; published online 15 December 2017)

We demonstrate theoretically and experimentally a plasmonic metasurface operating as a broadband polarization converter with adequate efficiency which can transform linearly polarized light into its orthogonal polarization in the near-infrared region. The unit cell of the specifically designed metasurfaces is composed of an asymmetric split-ring resonator (SRR) within a square metallic hole. The adequate polarization conversion rate arises from the enhancement of the cross-polarized electric field and the decrease in the co-polarized electric field induced by the symmetry breaking of the SRR. Furthermore, a broad operating frequency range results from the overlap of multiple polarization rotation responses, which are generated in the combined symmetry-breaking SRRs and square metallic holes. This ultrathin single-layer metasurface avoids the complicated fabrication process of multilayered and tridimensional polarization converters and offers more intriguing possibilities to design high-performance plasmonic metasurfaces for polarization modulation. *Published by AIP Publishing.* https://doi.org/10.1063/1.5006540

The manipulation of the polarization state of electromagnetic waves has attracted much attention because it can offer more chances to develop optical devices.[1] Conventional approaches to controlling the polarization state include half-wave plates,[2] birefringent crystals,[3] and optical active materials with Faraday effects,[4] which are usually bulky in size and bring much difficulty in miniaturization. Recently, metamaterials provided a potential way to manipulate the polarization state of light due to their outstanding advantage for nanophotonic integration. Metamaterials,[5] artificially designed with subwavelength meta-atoms, offer diverse potential applications due to their distinct electromagnetic performances, such as negative refraction,[6] perfect absorption,[7] and plasmon-induced transparency.[8]

In recent years, metamaterials have been demonstrated to realize optical activity which refers to the polarization rotation of linearly polarized light. There are three main approaches to realizing highly efficient polarization conversion. One of these approaches to showing optical activity behavior is three-dimensional photonic metamaterials,[9–11] such as gold-helix arrays[9] and meshed helical metamaterials.[10] Multi-layer structures consisting of different metasurface layers have been presented as another way to realize enhanced polarization rotation. The two-layer structures are the simplest multi-layer metamaterials to manipulate the polarization states of electromagnetic waves.[12,13,23] What's more, a three-layer metamaterial, composed of a chiral unit cell between two orthogonal gratings, is another typical method of multi-layer structures, serving as a high-performance cross polarization rotator.[14,15] Also, there exist twisted optical metamaterials designed with more than three ultrathin layers for broadband circular polarizers.[16,17] However, three-dimensional photonic metamaterials and multi-layer structures are both limited by complicated fabrication. The third method to observe polarization conversion is using single-layer metasurfaces,[18–22] specifically designed with perforated building blocks.[20,21] The perforated holes are usually chiral or have a broken symmetry, and they can not only support surface plasmon polaritons (SPPs) to enhance transmission but also motivate localized surface plasmons (LSPs) to achieve polarization rotation of incident light.[20] However, the combination of LSP resonances with SPP resonances results in narrow band conversion, which limits the polarization converters for practical applications.

In this letter, we design a broadband polarization converter in the transmission mode, which is based on ultrathin single-layer metasurfaces containing symmetry-breaking split ring resonators (SRRs) and square holes. The broadband transform effect is attributed to the overlap of multiple polarization rotation responses, which are generated in the combined symmetry-breaking SRRs and square metallic holes. By breaking the symmetry and changing the split gaps (δ) in the SRRs, the polarization state can be controlled efficiently. The experimental polarization conversion rate (PCR) over 70% could be sustained over a broad frequency range about 41 THz for the metasurface of $\delta = 200$ nm, which agrees well with simulation results. Based on simultaneous realization of the broadband response and adequate polarization conversion rate, our work provides the promising candidates for broadband cross-polarization conversion by ultrathin metasurfaces.

Here, we start by considering the theoretical analysis for the polarization conversion of linearly polarized light and deriving general expressions to characterize the conversion

[a)]Author to whom correspondence should be addressed: czgu@iphy.ac.cn

rate. The transmission of coherent light through any dispersive optical system can be expressed by the means of complex Jones matrices T.[24] The metasurfaces are illuminated by a plane wave propagating along the positive z direction, and the generally complex amplitudes of the incident field and the transmitted field can be related by the Jones matrix T,

$$\begin{pmatrix} E_t^x \\ E_t^y \end{pmatrix} = \begin{pmatrix} T_{xx} & T_{xy} \\ T_{yx} & T_{yy} \end{pmatrix} \begin{pmatrix} E_i^x \\ E_i^y \end{pmatrix}, \tag{1}$$

where E_i^x and E_i^y denote the complex amplitudes of incident waves, E_t^x and E_t^y denote the complex amplitudes of transmitted waves, and T_{ij} ($i, j = x, y$) represents i-polarized electric transmission from j-polarized incident light. In our designs, the polarization direction of the incident light is along the y-axis, and so, there exists $\begin{pmatrix} E_i^x \\ E_i^y \end{pmatrix} = \begin{pmatrix} 0 \\ 1 \end{pmatrix}$. Hence, the transmitted field can be described as

$$\begin{pmatrix} E_t^x \\ E_t^y \end{pmatrix} = \begin{pmatrix} T_{xy} \\ T_{yy} \end{pmatrix}. \tag{2}$$

Therefore, the polarization conversion rate (PCR) is defined as

$$PCR = \frac{t_x}{t_x + t_y} = \frac{|T_{xy}|^2}{|T_{xy}|^2 + |T_{yy}|^2}. \tag{3}$$

Here, the PCR is generally applied to characterize the optical activity. In order to obtain giant polarization conversion, the transmission matrix elements should satisfy the condition $|T_{xy}| > |T_{yy}|$. For the unit cell of the symmetric metasurface about the y-axis, it certainly satisfies the matrix operation: $\hat{D}_y = \begin{pmatrix} -1 & 0 \\ 0 & 1 \end{pmatrix}$. Thus, the new T matrix $\hat{T}_{new}$ can be given by $\hat{T}_{new} = D_y^{-1}\hat{T}D_y = \begin{pmatrix} T_{xx} & -T_{xy} \\ -T_{yx} & T_{yy} \end{pmatrix} \equiv \hat{T} = \begin{pmatrix} T_{xx} & T_{xy} \\ T_{yx} & T_{yy} \end{pmatrix}$. It distinctly indicates that the cross-polarization transmission matrix elements of the symmetric metasurface possess the following relation: $T_{xy} = T_{yx} = 0$. Theoretically, the above results indicate that the symmetric metasurfaces could not realize optical activity.

Based on the above theoretical analysis, we have designed a symmetry-breaking single-layer metasurface to realize the polarization conversion, as depicted in Fig. 1. The designed metasurfaces can transform a linearly polarized wave to its cross-polarized component and restrain co-polarized one as shown in Fig. 1(a). Figures 1(b) and 1(c) exhibit the schematic of the symmetric and asymmetric unit cells of proposed metasurfaces, respectively. The proposed metamaterial with unit cell period p = 800 nm is composed of asymmetric SRR (w = 100 nm and b = 200 nm) and a square metallic hole (a = 600 nm). The degree of asymmetry can be tuned by varying the split gap δ in the SRR from 0 to 300 nm. In the experiments, a 100 nm thick gold film is sputtered on the 0.5 mm thick quartz substrate. All the samples were fabricated using a focused ion beam system (Helios 600i). The scanning electron microscopy (SEM) image over a magnified area of $40 \times 40\ \mu m^2$ with $\delta = 200$ nm is shown in

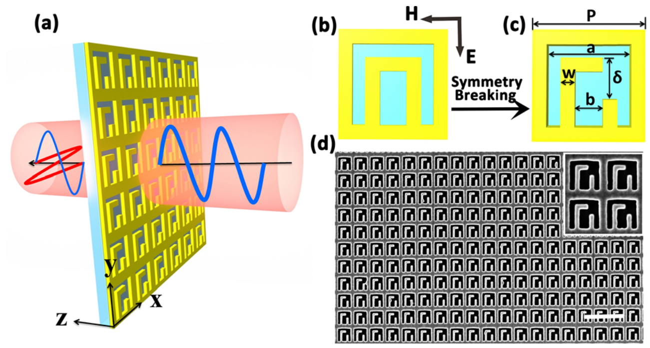

FIG. 1. Single-layer linear polarization converter. (a) An artistic rendering of polarization conversion for the designed ultrathin single-layer metasurface. The schematic of symmetric (b) and asymmetric (c) unit cells of proposed metasurfaces. (d) SEM image of a typical sample with $\delta = 200$ nm. The inset shows a magnified view with the metamaterial. The scale bar is 2 μm.

Fig. 1(d). The transmission spectra were measured by home-made optical measurement setups. In order to clarify the mechanism of the cross-polarized transmission spectra, numerical simulations were performed using the frequency domain solver of the commercial software CST Microwave Studio. In the simulation, the permittivity of bulk gold in the infrared spectral regime was described by the Drude model with the plasma frequency $\omega_{pl} = 2\pi \times 2.175 \times 10^{15}\ s^{-1}$ and the damping constant $\omega_c = 2\pi \times 6.5 \times 10^{12}\ s^{-1}$.[25] Taking the surface scattering and grain boundary effects in the thin gold film into account, the simulation results were obtained using a damping constant which was three times larger than that of the bulk material. Periodic boundary conditions on both x- and y-directions were applied to characterize the periodic structures, and an open boundary was imposed in the z-direction.

To study how the operating bandwidth and transmission of designed polarization converters are controlled by the parameter δ, the simulated cross-polarized (T_{xy}) and co-polarized (T_{yy}) amplitude transmission spectra are shown in Fig. 2. The parameter δ changes from 0 to 300 nm, and all the other parameters are constant. The f_1 and f_2 marked in Fig. 2(a) are two representative resonance frequencies of the simulated T_{xy} spectra, and we will analyze the evolution of surface electric field distributions at both f_1 and f_2 later. It appears distinctly that T_{xy} spectra could be tuned by varying the δ value. Extremely weak cross-polarized transmission is induced for the symmetric metasurface ($\delta = 0$ nm) as indicated in Fig. 2(a), which agrees well with theoretical predictions. When symmetry breaking is introduced to the ring resonator, strong optical activity appears. It can be noticed that the highest cross-polarized transmission amplitude for the case of $\delta = 200$ nm is 0.463, approaching to the theoretical limit 0.5 of the cross-polarized amplitude transmission in a single-layer metasurface.[26] As shown in Fig. 2, this device satisfies $|T_{xy}| > |T_{yy}|$ in a broad frequency range between 184.9 THz and 267.4 THz. Furthermore, the cross-polarization transmission for the metasurface of $\delta = 300$ nm is larger than 0.35 in a broad frequency range of 170.4–268.5 THz. The peak value and bandwidth of the T_{xy} spectra for the case of $\delta = 200$ nm are superior to those for the case of $\delta = 300$ nm.

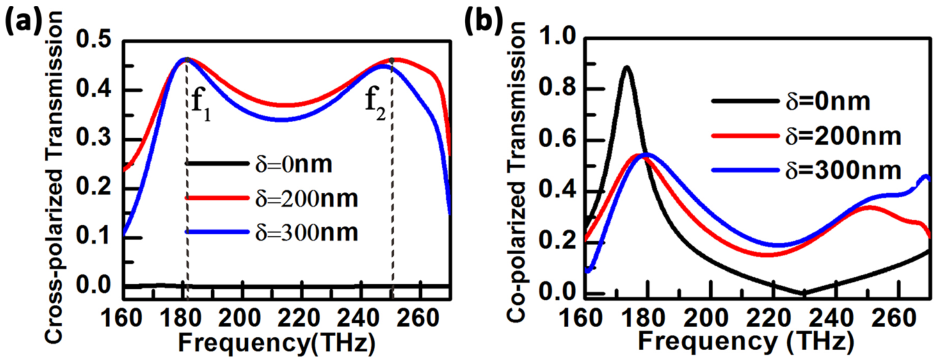

FIG. 2. The simulated cross-polarized (T_{xy}) (a) and co-polarized (T_{yy}) (b) amplitude transmission spectra for the asymmetric metasurfaces as δ is swept from 0 to 300 nm keeping the incident E field polarization fixed.

On the other hand, Fig. 2(b) shows that T_{yy} for both the cases of $\delta = 200$ nm and $\delta = 300$ nm is non-zero. The effect is reasonable because it has been theoretically proved that if the coupling to the cross-polarization is non-zero, the coupling to the co-polarization is required to be non-zero in a single metasurface.[26] That's to say, the polarization converter based on a single-layer metasurface is incapable of realizing complete polarization conversion. However, our proposed metasurfaces realize a broadband polarization conversion while taking into consideration of its satisfactory cross-polarization conversion as well.

In order to verify our previous simulation results, we have prepared and characterized several devices with different values of δ. In our experiments, the linearly polarized light along the y-axis was achieved via a linear polarizer and illuminated normally to the sample plane. The co-polarized transmission was collected when the polarization analyzer was parallel to the polarizer, while the cross-polarized transmission was obtained when the polarization analyzer was rotated for 90°. The optical transmission t_{ij} is the square of amplitude transmission $|T_{ij}|$. Transforming the optical transmission to amplitude transmission, we got the experimental cross-polarized and co-polarized amplitude transmission spectra for the proposed asymmetric metasurfaces as shown in Fig. 3. As observed in Fig. 3(a), the cross-polarized amplitude transmission T_{xy} is almost zero when

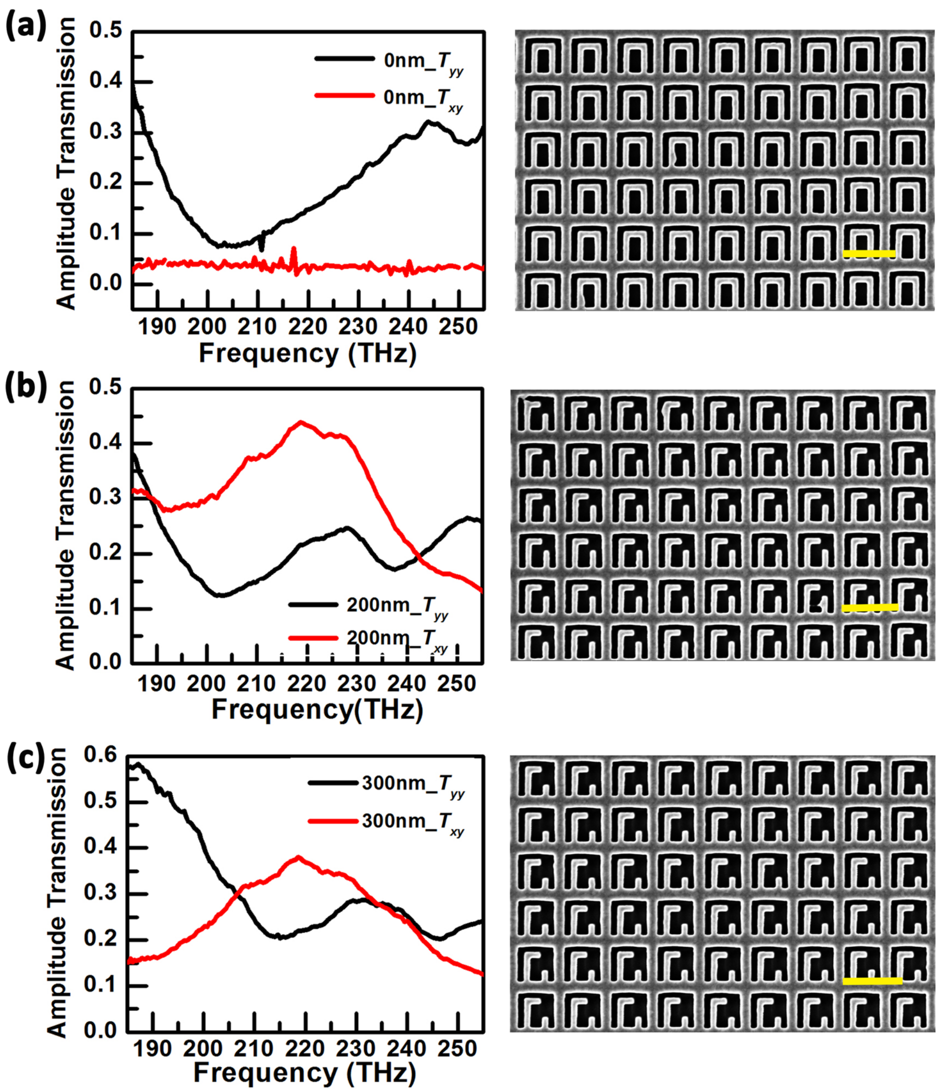

FIG. 3. Comparison of measured amplitude transmission T_{xy} and T_{yy} spectra for the device of $\delta = 0$ nm (a), $\delta = 200$ nm (b), and $\delta = 300$ nm (c) and the corresponding SEM images in the right; the scale bar is 1 μm.

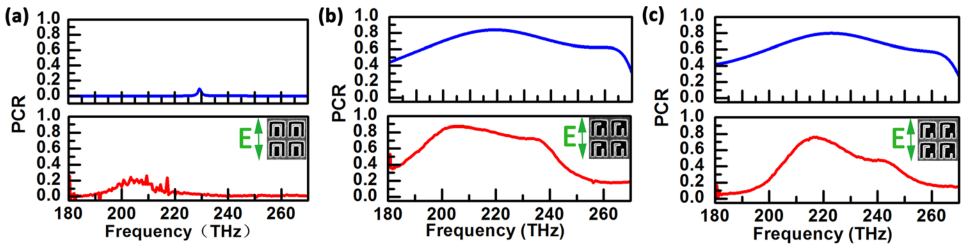

FIG. 4. The simulated (blue) and experimental (red) polarization conversion rate (*PCR*) spectra for the proposed metasurfaces when δ is swept from 0 to 300 nm (a)–(c). The inset shows the corresponding SEM images and incident electric field polarization.

$\delta = 0$, in which the nonzero intensity comes from the imperfect polarizer and the detector's noise. As shown in Fig. 3(b), the peak value of T_{xy} spectra when $\delta = 200$ nm is up to 0.44, and the frequency range of T_{xy} higher than 0.3 is at 200.3–234.1 THz, indicating the broadband polarization conversion. The experimentally measured curves are consistent with the numerically simulated curves although the additional absorption losses from the gold film and quartz substrate reduce the peak value and bandwidth of the cross-polarized transmission. As shown in Fig. 3(c), the peak value of T_{xy} reaches to 0.4, and the difference of cross-polarized and co-polarized transmission is not remarkable for the device of $\delta = 300$ nm. Although T_{yy} is theoretically required to be non-zero, it is small enough to satisfy $|T_{xy}| > |T_{yy}|$ in a broad frequency range of 189.0–242.1 THz for the case of $\delta = 200$ nm. Despite the existence of some unwanted absorption losses and an imperfect polarization analyzer in our experiments, the proposed single-layer metasurfaces still could operate as a broadband linear polarization converter, particularly when $\delta = 200$ nm.

To intuitively characterize the polarization conversion of asymmetric metasurfaces, the simulated and experimental polarization conversion rate (*PCR*) spectra for different split gaps in the SRR are shown in Fig. 4. Because almost no cross polarization light is induced for the metasurface of $\delta = 0$ nm, which is shown in Fig. 2(a) and theoretical analysis, the PCR is almost zero theoretically and experimentally. A weak peak is clearly observed in experimental *PCR* spectra at the frequency of about 203 THz, attributed to the minimum value of measured T_{yy} spectra at the same frequency, as shown in Fig. 3(a). The same phenomenon also occurs in the simulated *PCR* spectra. Once the symmetry of SRR is broken, large polarization conversion appears as shown in Figs. 4(b) and 4(c). The simulated *PCR* spectrum in Fig. 4(b) indicates that over 70% of the energy of the transmitted wave converts into the cross-polarized component for the case of $\delta = 200$ nm in the range of 200.1–240.6 THz, while the corresponding frequency range in the experiment is 195.3–236.4 THz. Based on above-mentioned experimental results, the polarization conversion over 70% could be sustained over a broad frequency range about 41 THz for the metasurface of $\delta = 200$ nm. Due to the fabrication tolerance and additional losses of the metallic film and quartz substrate, the operating frequency ranges in the experiments are red-shifted and not as wide as those in the simulations. However, the measured PCR spectra possess a significant peak value up to 87.1%. For the metasurface of $\delta = 300$ nm, both the peak value and working frequency range are inferior to the metasurface of $\delta = 200$ nm. In terms of the peak value and bandwidth of PCR spectra, the incident polarization state of the proposed asymmetry metasurfaces could be manipulated efficiently when $\delta = 200$ nm.

In order to elucidate the underlying physics of the observed spectral characteristics of the proposed asymmetric metasurfaces, we analyzed the evolution of the surface electric field distribution in both x and y directions at 181.82 THz (f_1) and 251.78 THz (f_2), as shown in Fig. 5. The electric field distributions are closely dependent on the parameter δ; thus, we take the electric field distributions of the symmetric metasurface as a comparison. Here, the E_x intensity of the symmetric metasurface is symmetric about the y-axis at both f_1 and f_2. The left and right parts possess a phase difference of π, resulting in complete reciprocal inhibition. Thus, no cross-polarized transmission is observed for the symmetric metasurface, as predicted in Fig. 2(a). As shown in Fig. 5(a), for the asymmetric metasurface, the E_x distributions at f_1 in zone (1) and zone (2) remain the same phase, thus leading to mutual promotion, which is important to the polarization rotation in single-layer metasurfaces. As shown in Fig. 5(b), the E_x distributions of zone (5) and (7) at f_2 possess equivalent electric field intensity and a different phase of π, leading to reciprocal inhibition. However, the presence of the stronger electric field E_x in zone (6) results in high polarization conversion at f_2. By contrast, a phase difference of π exists in zones (3) and (4) of the E_y components at f_1, which weakens the summation of E_y on the surface, further leading to the decrease in T_{yy}. This situation also exists in zones (8) and (9) of the E_y components at f_2. The results show that the symmetry breaking of SRR could generate the electric field perpendicular to the incident one, and it is a vital precondition for realizing polarization conversion. Furthermore, partial symmetry of the designed structure leads to the suppression of the co-polarized component, which could improve the polarization conversion rate. It can be inferred from the above analysis that the asymmetric metasurface ($\delta = 200$ nm) could achieve polarization conversion at more different frequencies. More than one response of polarization conversion overlaps, contributing to the broadband cross polarization conversion.

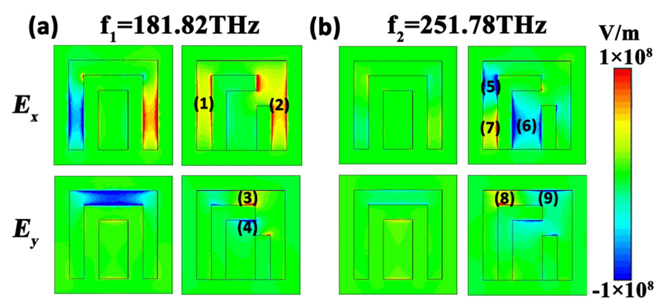

FIG. 5. Near-field E_x and E_y distributions at f_1 (a) and f_2 (b) on the surface of the symmetric and asymmetric metasurfaces ($\delta = 200$ nm), respectively.

In conclusion, we have demonstrated the broadband cross polarization transmission response of the asymmetric metasurfaces theoretically and experimentally. The unit cell of the metasurface-based polarization converters is a single-layer asymmetric SRR within the metallic square hole. The adequate linear polarization conversion rate results from the simultaneous presence of broken symmetry and partial symmetry in the unit cell. Through the overlap of more than one response of polarization conversion generated in the combined asymmetric SRRs and square holes, the broadband cross-polarized transmission has been realized, which can be efficiently tuned by the split gap of SRR in the near-infrared spectrum. Such an efficient single-layer polarization converter considerably enriches the variety of transmission functionalities, and its simple preparation process offers a promising future for the design on integrated photonic devices.

This work was supported by the National Key Research and Development Program of China (Grant Nos. 2016YFA0200400 and 2016YFA0200800), the National Natural Science Foundation of China (Grant Nos. 91323304, 11674387, 11504414, 11574369, 11574385, 11574368, and 61390503), and the Strategic Priority Research Program of the Chinese Academy of Sciences (Grant No. XDB07020200).

[1]A. Papakostas, A. Potts, D. M. Bagnall, S. L. Prosvirnin, H. J. Coles, and N. I. Zheludev, Phys. Rev. Lett. **90**, 107404 (2003).
[2]C. J. Koester, J. Opt. Soc. Am. **49**, 405 (1959).
[3]J. R. L. Moxon, A. R. Renshaw, and I. J. Tebbutt, J. Phys. D: Appl. Phys. **24**, 1187 (1991).
[4]W. Kaminsky and E. Hartmann, Z. Phys. B **90**, 47 (1993).
[5]D. R. Smith and J. B. Pendry, Opt. Soc. Am. B **23**, 391 (2006).
[6]T. Ergin, N. Stenger, P. Brenner, J. B. Pendry, and M. Wegener, Science **328**, 337 (2010).
[7]N. I. Landy, S. Sajuyigbe, J. J. Mock, D. R. Smith, and W. J. Padilla, Phys. Rev. Lett. **100**, 207402 (2008).
[8]S. Yang, X. Xia, Z. Liu, E. Yiwen, Y. Wang, C. Tang, W. Li, J. Li, L. Wang, and C. Gu, J. Phys. Condens. Matter **28**, 445002 (2016).
[9]J. K. Gansel, M. Thiel, M. S. Rill, M. Decker, K. Bade, V. Saile, G. v. Freymann, S. Linden, and M. Wegener, Science **325**, 1513 (2009).
[10]H. S. Park, T.-T. Kim, H.-D. Kim, K. Kim, and B. Min, Nat. Commun. **5**, 5435 (2014).
[11]S. Zhang, J. Zhou, Y. S. Park, J. Rho, R. Singh, S. Nam, A. K. Azad, H. T. Chen, X. Yin, A. J. Taylor, and X. Zhang, Nat. Commun. **3**, 942 (2012).
[12]R. Zhao, L. Zhang, J. Zhou, T. Koschny, and C. M. Soukoulis, Phys. Rev. B **83**, 035105 (2011).
[13]Y. Cui, L. Kang, S. Lan, S. Rodrigues, and W. Cai, Nano Lett. **14**, 1021 (2014).
[14]C. Pfeiffer, C. Zhang, V. Ray, L. J. Guo, and A. Grbic, Phys. Rev. Lett. **113**, 023902 (2014).
[15]N. K. Grady, J. E. Heyes, D. R. Chowdhury, Y. Zeng, M. T. Reiten, A. K. Azad, A. J. Taylor, D. A. R. Dalvit, and H. T. Chen, Science **340**, 1304 (2013).
[16]Z. Wei, Y. Cao, Y. Fan, X. Yu, and H. Li, Appl. Phys. Lett. **99**, 221907 (2011).
[17]Y. Zhao, M. A. Belkin, and A. Alù, Nat. Commun. **3**, 870 (2012).
[18]L. Cong, Y. K. Srivastava, and R. Singh, Adv. Opt. Mater. **4**, 848 (2016).
[19]M. Kuwata-Gonokami, N. Saito, Y. Ino, M. Kauranen, K. Jefimovs, T. Vallius, J. Turunen, and Y. Svirko, Phys. Rev. Lett. **95**, 227401 (2005).
[20]S. Wu, Z. Zhang, Y. Zhang, K. Zhang, L. Zhou, X. Zhang, and Y. Zhu, Phys. Rev. Lett. **110**, 207401 (2013).
[21]W. Liu, S. Chen, Z. Li, H. Cheng, P. Yu, J. Li, and J. Tian, Opt. Lett. **40**, 3185 (2015).
[22]E. Plum, V. A. Fedotov, and N. I. Zheludev, Appl. Phys. Lett. **108**, 141905 (2016).
[23]K. Hannam, D. A. Powell, I. V. Shadrivov, and Y. S. Kivshar, Phys. Rev. B **89**, 125105 (2014).
[24]C. Menzel, C. Rockstuhl, and F. Lederer, Phys. Rev. A **82**, 053811 (2010).
[25]M. A. Ordal, L. L. Long, R. J. Bell, S. E. Bell, R. R. Bell, R. W. Alexander, Jr., and C. A. Ward, Appl. Opt. **22**, 1099 (1983).
[26]F. Monticone, N. M. Estakhri, and A. Alù, Phys. Rev. Lett. **110**, 203903 (2013).